UNSTEADY PROPULSIVE CHARACTERISTICS OF BIOFOILS MOVING IN A VERY LOW-REYNOLDS NUMBER FLOW

Cheol-Heui Han*, Sang-Joon An, Joo-Sung Maeng****
***Chungju National University, ****Hanyang University**

Keywords: *Thust Generation, Biomimetic Foil, Lattice Boltzmann Method*

Abstract

Unsteady propulsive characteristics of biofoils are investigated using a lattice-Boltzmann method. The biofoils are assumed to move in the low Reynolds number flow (5<Re<100). It is found that a wiggling foil and a heaving foil with deflection are promising propulsors for vehicles moving in a low Reynolds number flow. The results from this study can be applied to the design of micro flapping propulsor systems for aeronautical or biomedical use.

1 Introduction

Birds and insects flap their wings to fly through the stationary air. Big birds flap their wings with low frequency, whereas small birds or insects flap their wings with high frequency. The smaller the body size, the higher the frequency of the flapping wings. Thus, it can be conjectured from the fact that the flapping propulsion is not so effective when the body sizes of the creatures are small. The observation of the sea angels of the family Clionidae clearly shows that they change the mode of locomotion from ciliary to flapping propulsion according to the Reynolds number[1].

With the progress of sensors and actuators based on the micro-electro-mechanical system technology, it is possible to fabricate a very small-size vehicle such as a nano air vehicle(NAV). According to DARPA, the vehicle's span should be less than 2 inch and its take-off gross weight should also be lighter than 12g[2]. In the biomedical engineering field, a nano robot with extremely small size has been suggested. To construct the extremely small vehicle, it is important to understand the unsteady propulsive characteristics of a foil moving in a low Reynolds number flow where viscous force dominates other forces and, accordingly, flapping motions can be ineffective for propulsion [1].

It is still questionable that the thrust can be generated in a microscale (low Reynolds number, Re<100) as it can in a macro scale (in general 1,000<Re<500,000). It is also curious what types of foils are more effective than the others in generating the thrust force in the low Reynolds number flow. Thus, in this paper, four kinds of biomimetic foils (biofoils) are selected and studied for their thrust generation capabilities. A lattice-Boltzmann method developed by considering a moving boundary condition is utilized to investigate the propulsive characteristics of the biofoils. Present method was validated by comparing computed results with the aerodynamic characteristics data of stationary and oscillating cylinders[3]. The effect of the changes in the Strouhal and Reynolds numbers on the thrust generation is discussed focused on the onset of thrust force generation

2 Numerical Methods

2.1 Lattice Boltzmann Methods

The Boltzmann equation is represented as

$$\frac{\partial f}{\partial t} + \vec{e} \cdot \vec{\nabla} f = Q \qquad (1)$$

where f is a single-particle distribution function, Q is the collision integral, and $\vec{e}$ is the velocity of a particle. Starting from the initial state, the

configuration of particles at each time step evolves in two sequential sub-steps; the first step is streaming, in which each particle moves to the nearest node of velocity direction. The second step is collision, which occurs when particles arrive at a node, interact, and then change their velocity directions according to scattering rules. Both left-hand side and the right-hand side of eq. (1) represents streaming and collision process, respectively. The collision operator (Q) can be simplified using the BGK approximation of Bhatnagar, Gross, and Krook [4,5]:

$$\frac{\partial \mathrm{f}}{\partial \mathrm{t}} + \vec{\mathrm{e}} \cdot \vec{\nabla} \mathrm{f} = -\frac{1}{\tau}(\mathrm{f} - \mathrm{f}^{\mathrm{eq}}) \qquad (2)$$

where f^{eq} is the local equilibrium distribution function, τ is the relaxation time for collisions, and $\vec{e}$ denotes the discrete velocity set as next,

$$\begin{array}{ll} c(0,0) & i=0 \\ c(\cos\theta_i, \sin\theta_i), \quad \theta_i = (i-4)\pi/2\,, & i=1-4 \\ \sqrt{2}c(\cos\theta_i, \sin\theta_i), \ \theta_i = (i-4)\pi/2 + \pi/2, & i=5-8. \end{array} \qquad (3)$$

the subscript, i represents the direction of the discrete velocity, and $c \equiv \delta x / \delta t$, with δx and δt being the lattice size and the time-step size, respectively. The local equilibrium distribution, f_i^{eq}, is the form of

$$f_i^{eq} = w_i \rho [1 + 3\frac{\vec{e_i} \cdot \vec{u}}{c^2} + \frac{9}{2}\frac{(\vec{e_i} \cdot \vec{u})^2}{c^4} - \frac{3}{2}\frac{\vec{u} \cdot \vec{u}}{c^2}] \qquad (4)$$

where the weighting factor, w_i, is given

$$w_i = \begin{cases} 4/9, & i=0 \\ 1/9, & i=1-4 \\ 1/36, & i=5-8. \end{cases} \qquad (5)$$

For the particle distribution function, the macroscopic quantities, the density and the velocity, can be given by

$$\rho = \sum_{i=0}^{8} f_i \qquad (6)$$

$$\vec{u} = \frac{1}{\rho}\sum_{i=0}^{8} f_i \vec{e}_i \qquad (7)$$

Using the Chapman-Enskog multi scale expansion technique [6], we attain the second-order Navier-Stokes equation. Therefore, the kinematic viscosity and pressure are given

$$\nu = \frac{2\tau - 1}{6} \qquad (8)$$

$$p = \rho \cdot C_s^{\,2} \qquad (9)$$

where sound speed , $c_s = c/\sqrt{3}$.

2.2 Moving Boundary Condition

Two-dimensional biomimetics foils move at each lattice time with their motions. A moving boundary condition [7] is applied to a D2Q9 lattice Boltzmann model in order to represent the added force and no-slip condition on the lattice points and surface boundaries. The moving boundary condition is composed of the ratio (q) of the fluid territory to the solid territory in between the fluid-solid boundary lattices. With the known ratio of q, the equation is set in nine distributed directions with the moving velocity on the plates.

$$\begin{aligned} f_i(\vec{x},t) = {} & q(1+2q) f_i(\vec{x} + \vec{e}_i\delta t, t) + (1-4q^2) f_i(\vec{x},t) \\ & - q(1-2q) f_i(\vec{x} - \vec{e}_i\delta t, t) + 6w_i(\vec{e}_i \cdot \vec{u}_w), \quad q < \frac{1}{2} \end{aligned} \qquad (10a)$$

$$\begin{aligned} f_i(\vec{x},t) = {} & \frac{1}{q(2q+1)} f_i(\vec{x} + \vec{e}_i\delta t, t) + \frac{(2q-1)}{q} f_i(\vec{x} - \vec{e}_i\delta t, t) \\ & - \frac{(2q-1)}{(2q+1)} f_i(\vec{x} - 2\vec{e}_i\delta t, t) + \frac{6w_i}{q(2q+1)}(\vec{e}_i \cdot \vec{u}_w), \quad q \geq \frac{1}{2} \end{aligned} \qquad (10b)$$

where f_i is the distribution function of a moving particle with $\vec{e}_i (\equiv -\vec{e}_i)$ and the wall velocity of the plate, $\vec{u}_w$. When a solid lattice point is changed into a fluid lattice point, the distribution function (f_i) is determined by second order extrapolation [7] using the nearest fluid lattice points which are perpendicular to the plate surface.

2.3 Code Validation

Present method is validated for a flexible foil

by comparing the time-averaged thrust coefficients with the results calculated by using a Navier-Stokes equation solver with conformal hybrid mesh system by Miao and Ho[8]. They studied the thrust characteristics of a flexible foil at 100≤ Re≤ 10,000. Reynolds number and Strouhal number are defined as follows,

$$\mathrm{Re} = \frac{U \cdot C}{\nu} \tag{11}$$

$$St_a = \frac{f \cdot 2h}{U} \tag{12}$$

where U is free-stream velocity, C is chord length of the foil, f is heaving frequency, and h is heaving amplitude. As shown in Fig. 1, the present results agree well with the published data [8].

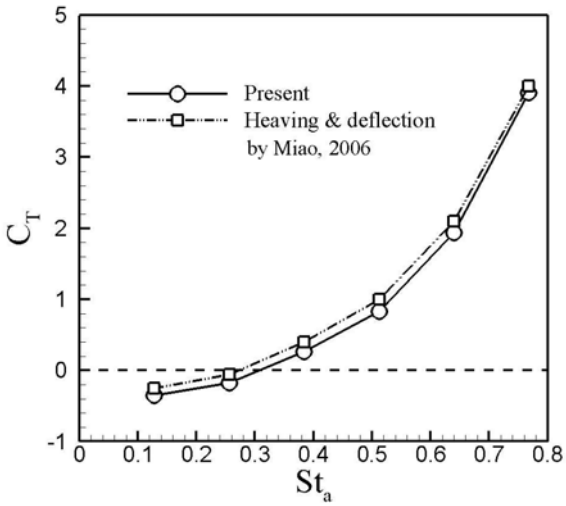

Fig. 1. Comparison of the present results with those by N-S computations for a flexible foil moving at Re=100

3 Results and Discussions

3.1 Nomenclature

To investigate the effective propulsors moving in a low Reynolds number flow, four kinds of biomimetic foils are selected and their propulsive characteristics are calculated at Re=5 and Re=100 by changing the Strouhal number.

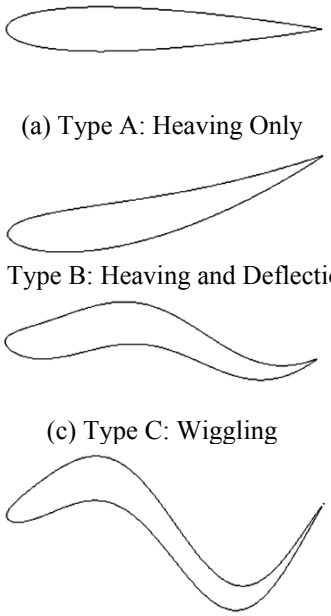

(a) Type A: Heaving Only

(b) Type B: Heaving and Deflection

(c) Type C: Wiggling

(c) Type D: Undulation

Fig. 2. Biomimetic foils in the present study

The four foils have the airfoil shape of NACA 0012. Two foils (Type A and Type B) are undergoing a heave oscillation. The first foil is a base foil oscillating with a following kinematic equation,

$$y_c(t) = h\cos(\omega t) \tag{13}$$

where y_c is the mean camberline of the foil, h is the heave amplitude, and ω is the angular velocity of the heave oscillation. The second foil deflects its whole parts with the amplitude of c_0 and the phase difference of Φ to the heave oscillation.

$$y_c(x,t) = \frac{c_0}{C}x^2\cos(\omega t + \phi) \tag{14}$$

The third and fourth foils (Type C and Type D) are undergoing wiggling and undulation motions, respectively. The motions can be represented as follows.

Wiggling:

$$y_c(x,t) = a_0 C[-(\frac{x}{C}-1)^2 + 1]\cos 2\pi/\lambda(x-ct) \tag{15}$$

Undulation:

$$y_c(x,t) = a_m(x)\cos(2\pi x/\lambda - 2\pi ft) \tag{16}$$

$$a_m(x) = a_1 + a_2 x + a_3 x^2 + a_4 x^3 \qquad (17)$$

where λ is the wave length, c is the phase speed, f is the frequency. a_0 and a_m are the amplitudes of wiggling and undulation, respectively. Table 1 represents the values of parameters that are used in this study.

Table 1 Values of the kinematic parameters of the present study

h	c_0	Φ	c	λ
0.243C	0.3C	$-\frac{\pi}{2}$	1.0	1.0
a_0	a_1	a_2	a_3	a_4
0.1	0.055306	0.22649	0.29446	0.32656

3.2 Re=5

In Fig. 3, the time-averaged thrust coefficients of four foils moving at Re=5 are plotted by changing the Strouhal number. It is shown in the figure that the heaving foil with deflection (Type B) generates larger thrust than the other types of foils at the same Strouhal number. The wiggling foil generates larger thrust than the Type A foil, which shows that the wiggling can be one of available propulsors for a vehicle moving in the low Reynolds number flow.

Fig. 4 shows the vorticity contours around the foils. As shown in the figure, vortices around the leading edges of heaving foils (Type A and Type B) are forming with their sizes almost equal to those in the nascent of the trailing edges. The deflection of the Type A foil effectively switches the signs of the vortices convected from the trailing edge while breaking the symmetry between the leading edge vortex and the trailing edge vortex. Comparing the wake shapes of the wiggling foil (Type C) with those of the undulatory foil (Type D), it can be deduced that the Type C foil can produce larger thrust that the Type D foil. The wake shapes behind the Type C foil is thrust-producing, whereas the wake shapes of the Type D foil is drag-producing. Notice that the wiggling motion is one of typical motions used by creatures moving in a very low Reynolds number flow, whereas the undulation is common to the fish moving in an intermediate or high Reynolds number flow. The undulatory foil does not produce the thrust even when its Strouhal number is larger than 1.6.

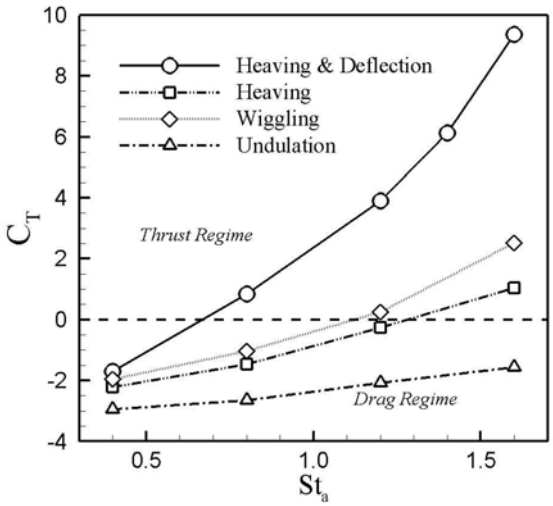

Fig. 3. Thrust coefficient for biomimetic foils at Re=5

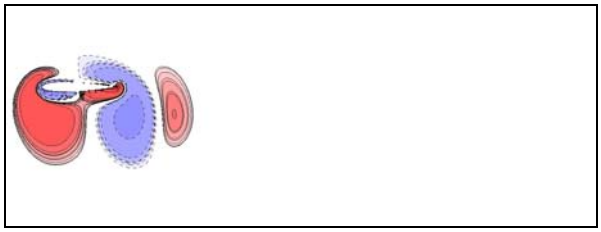

(a) heaving

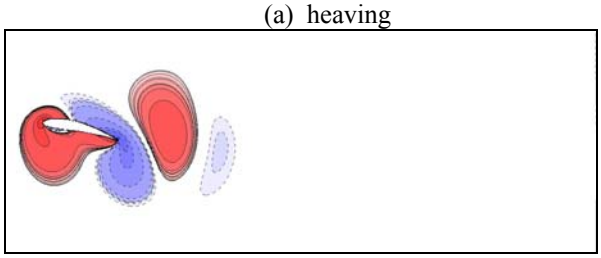

(b) heaving and deflection

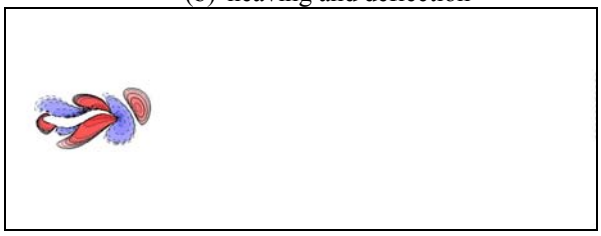

(c) wiggling

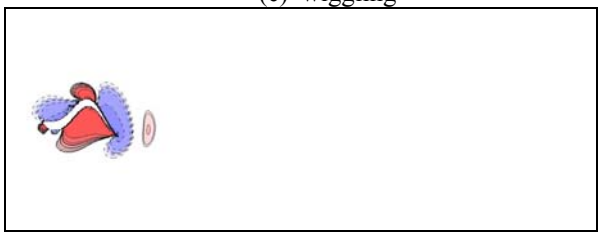

(d) undulation

Fig. 4. Vorticity contours at Re=5 in biomimetic foils (St_a=1.6)

3.3 Re=100

Fig. 5 shows the time-averaged thrust coefficients of the four foils moving at Re=100. It is shown in the figure that the thrust of the Type A foil is generated at approximately St_a=0.35. It is within the range of natural creature's Strouhal numbers($0.2 \le St_a \le 0.4$) for their efficient locomotion. The heaving foils (Type A and Type B) produces larger thrust at the same Strouhal number than the foils of Type C and Type D. The Type D foil do not generate thrust within the current calculated range of $St_a \le 0.8$. Comparing the results at Re=5 with those at Re=100, it can be said that the Type B foil produces larger thrust than the Type C, so the heaving foils are, in the aspect of thrust generation, more effective than the wiggling and undulatory foils at Re=100.

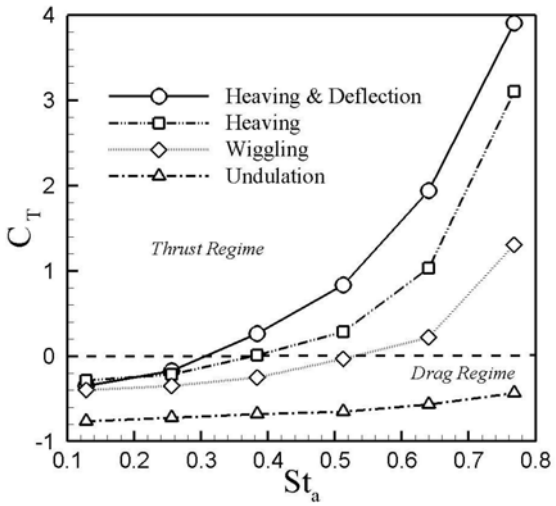

Fig. 5. Thrust coefficient for biomimetic foils at Re=100.

As shown in Fig. 6, at St_a =0.512, inverse Karman vortex streets are clearly observed in the heaving foils of Type A and Type B. The wake shapes behind the Type C foil is shown to initiate the formation of the inverse Karman vortex streets, whereas the wake shapes behind the Type D foil is the Karman vortex streets. For all the foils, broad regions of vorticity are spread out in the upper and lower surfaces of the foils. In case of the heaving foils and the wiggling foil, the trailing edges of the foils have the effect of changing the positions of the vortices into the opposite sides. However, in case of the undulatory foil, the positions of the vortices behind the foil remains at the same side, which results in the Karman vortex streets. As the Strouhal number increases, the trailing edge

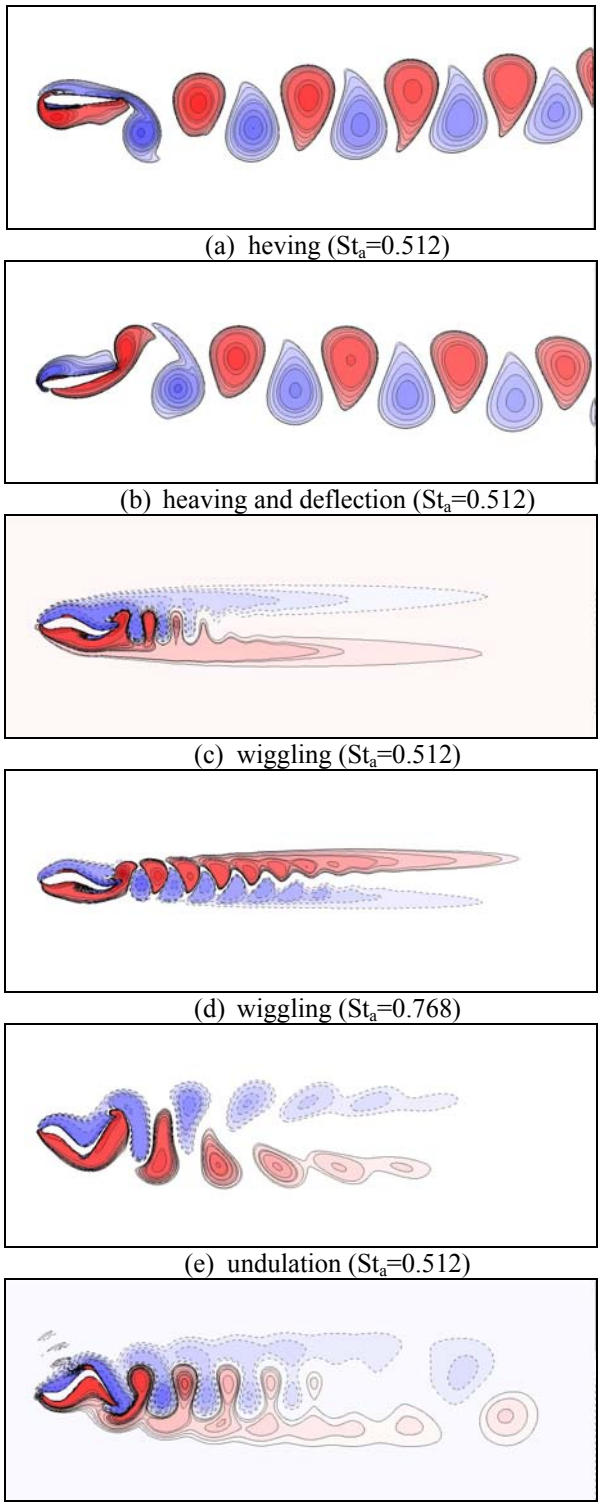

(a) heving (St_a=0.512)

(b) heaving and deflection (St_a=0.512)

(c) wiggling (St_a=0.512)

(d) wiggling (St_a=0.768)

(e) undulation (St_a=0.512)

(f) undulation (St_a=0.768)

Fig. 6. Vorticity contours at Re=100.

of the wiggling foil has an effect of changing the positions of the vortices, whereas the trailing edge of the undulatory foil cannot change the positions of the wake vortices completely.

4 Conclusions

The propulsive characteristics of the four types of biofoils moving in a low Reynolds number flow are investigated by employing the lattice Boltzmann method. The time-averaged thrust and the vorticity contours around the biofoils moving at Re=5 and Re=100 are compared with each other by changing the Strouhal number. It is found that, for both Re=5 and 100, the heaving foil with deflection is the most effective propulsor than any other foils. When the Reynolds number is equal to 5, it is found that the wiggling motion is more effective than the heaving foil without deflection. When the foils are moving at Re=100, the heaving foils generate larger thrust than the wiggling and undulatory foils. It is found that the motion of the trailing edge of the foil play a critical role in deciding if the foil produce thrust or drag. The vorticity contours around the foils show that the inverse Karman vortices are formed behind the thrust-producing biofoils, whereas the Karman or neutral vortex streets are shown behind the drag-producing foils.

References

[1] Childress S Dudley R. Transition from Ciliary to Flapping Mode in a Swimming Mollusc:Flapping Flight as a Bifurcation in Re_w. *Journal of Fluid Mechanics*, Vol. 498, pp. 257-288, 2004.

[2] An, S J., Maeng, J S., Han, C. Thrust Generation by Flapping Plates in a Very Low-Reynolds Number Flow, 2006 JSASS-KSAS Joint International Symposium on Aerospace Engineering, Oct. 12-14, 2006, Japan

[3] He, R Sato, S Drela M, Design of a Single-Motor Nano Aerial Vehicle with a Gearless Torque-Canceling Mechanism, 46th AIAA Aerospace Sciences Meeting and Exhibit, 7-10 January 2008, Reno, Nevada.

[4] Koelman J M V A. A Simple Lattice Boltzmann Scheme for Navier-Stokes Fluid Flow. *Eruophys. Lett.*, Vol. 15, No. 6, pp.603-607, 1991.

[5] Qian Y H d'Humieres D Lallemand P. Lattice BGK Models for Navier Stokes Equation. *Europhys. Lett.*, Vol. 17, No. 6, pp. 479-484.

[6] Chapman S. On the law of Distribution of Molecular Velocities, and on the Theory of Viscosity and Thermal Conduction, in a Non-uniform Simple Monatomic Gas. *Philosophical Transactions of Royal Society of London*, Vol. A216, pp. 279-348, 1916.

[7] Lallemand P Luo L. Lattice Boltzmann Method for Moving Boundaries. *Journal of Computational Physics*, Vol. 184, pp. 406-421, 2003.

[8] Miao J -M Ho M -H. Effect of Flexure on Aerodynamic Propulsive Efficiency of Flapping Flexible Airfoil. *Journal of Fluids and Structures,* Vol. 22, pp. 401-419, 2006.

Copyright Statement